



Article

Plasma-Enhanced Chemical Looping Oxidative Coupling of Methane through Synergy between Metal-Loaded Dielectric Particles and Non-Thermal Plasma

Shunshun Kang^{1,2,3,4}, Jinlin Deng^{1,2,3,4}, Xiaobo Wang^{1,2,3,4}, Kun Zhao^{1,2,3,4,*}, Min Zheng⁵ , Da Song^{1,2,3,4}, Zhen Huang^{1,2,3,4}, Yan Lin^{1,2,3,4} , Anqi Liu^{1,2,3,4}, Anqing Zheng^{1,2,3,4,*} and Zengli Zhao^{1,2,3,4}

¹ Guangzhou Institute of Energy Conversion, Chinese Academy of Sciences, Guangzhou 510640, China

² CAS Key Laboratory of Renewable Energy, Guangzhou 510640, China

³ Guangdong Provincial Key Laboratory of New and Renewable Energy Research and Development, Guangzhou 510640, China

⁴ University of Chinese Academy of Sciences, Beijing 100049, China

⁵ State Key Laboratory of Complex Metal Resources Clean Utilization, Kunming University of Science and Technology, Kunming 650031, China

* Correspondence: zhaokun@ms.giec.ac.cn (K.Z.); zhengaq@ms.giec.ac.cn (A.Z.);

Tel.: +86-0208-7057-716 (K.Z. & A.Z.); Fax: +86-0208-7057-737 (K.Z. & A.Z.)

Abstract: A plasma–catalyst hybrid system has been developed for the direct conversion of methane to C₂₊ hydrocarbons in dielectric barrier discharge (DBD) plasma. TiO₂ presented the highest C₂₊ yield of 11.63% among different dielectric materials when integrated with DBD plasma, which made us concentrate on the TiO₂-based catalyst. It was demonstrated that MnTi catalyst showed the best methane coupling performance of 27.29% C₂₊ yield with 150 V applied voltage, without additional thermal input. The catalytic performance of MnTi catalyst under various operation parameters was further carried out, and different techniques, such as X-ray diffraction, X-ray photoelectron spectroscopy, transmission electron microscopy, and H₂-temperature-programmed reduction were used to explore the effect of Mn loading on methane oxidative coupling (OCM) performance. The results showed that applied voltage and flow rate had a significant effect on methane activation. The dielectric particles of TiO₂ loaded with Mn not only synergistically affected the coupling reaction, but also facilitated charge deposition to generate a strong local electric field to activate methane. The synergy effects boosted the OCM performance and the C₂₊ yield became 1.25 times higher than that of the undoped TiO₂ under identical operating conditions in plasma, which was almost impossible to occur even at 850 °C on the MnTi catalyst in the absence of plasma. Moreover, the reaction activity of the catalyst was fully recovered by plasma regeneration at 300 °C and maintained its stability in for at least 30 consecutive cyclic redox tests. This work presents a new opportunity for efficient methane conversion to produce C₂₊ at low temperatures by plasma assistance.

Keywords: oxidative coupling of methane; chemical looping; synergy effects; plasma enhancement



Citation: Kang, S.; Deng, J.; Wang, X.; Zhao, K.; Zheng, M.; Song, D.; Huang, Z.; Lin, Y.; Liu, A.; Zheng, A.; et al. Plasma-Enhanced Chemical Looping Oxidative Coupling of Methane through Synergy between Metal-Loaded Dielectric Particles and Non-Thermal Plasma. *Catalysts* **2023**, *13*, 557. <https://doi.org/10.3390/catal13030557>

Academic Editors: Jong Wook Bae and Jean-François Lamonier

Received: 9 January 2023

Revised: 27 February 2023

Accepted: 3 March 2023

Published: 10 March 2023



Copyright: © 2023 by the authors. Licensee MDPI, Basel, Switzerland. This article is an open access article distributed under the terms and conditions of the Creative Commons Attribution (CC BY) license (<https://creativecommons.org/licenses/by/4.0/>).

1. Introduction

Light olefins, especially ethylene, are important organic raw materials, which are widely used in the production of plastics, drugs, fibers, etc. Ethylene is also regarded as a leading indicator in measuring the level of a country's petrochemical industry and plays a pivotal role in the national economy. Because of its abundant reserves and clean characteristics [1,2], it is considered that methane will replace oil as the primary energy in the future. Therefore, a significant amount of manpower and material resources have been invested in the comprehensive utilization of natural gas [3–5]. The production of low-carbon olefins from methane has attracted the attention of researchers [6]. The oxidative coupling of methane (OCM) offers a feasible approach for the direct conversion of methane to hydrocarbons [7–9]. However, because of the high reactivity of oxygen, which easily

reacts with reactants and products, the generation of by-products of CO and CO₂ at high temperatures is unavoidable, and the C₂₊ yield of the OCM reaction is still limited to no more than 30%; thus, it is difficult to provide economic benefits in industry. On this basis, a replaceable technique known as chemical looping oxidative coupling of methane (CL-OCM) is investigated. As shown in Figure 1, the main advantage of CL-OCM is the replacement of gaseous oxygen with lattice oxygen in the catalyst (also known as the oxygen carrier), thus avoiding an excessive oxidation of methane. CL-OCM has become a hot research topic, since it can attain a higher C₂ yield (between 20 and 30%) compared to traditional methods, including the direct conversion of methane and the non-oxidative coupling of methane (NCM) [10]. However, CL-OCM typically requires high-temperature reaction conditions due to the high C–H bond activation barrier of methane, resulting in a low catalyst stability and a high energy consumption. Therefore, it is necessary to develop more modest technologies to assist the CL-OCM strategy.

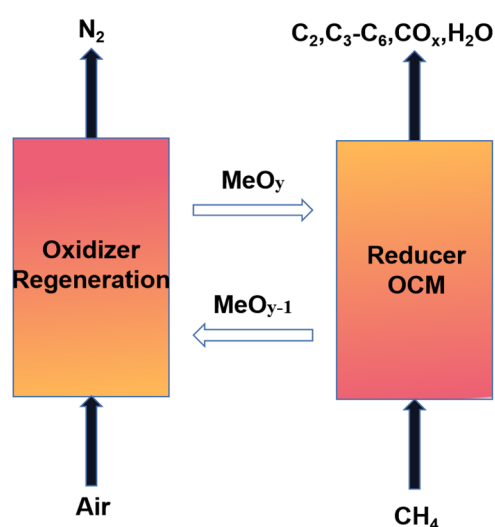


Figure 1. CL-OCM process.

As a system containing high-energy electrons and exhibiting low-temperature properties, plasma can effectively activate stable molecules at relatively low temperatures, thus providing a new approach toward CL-OCM. Plasma can be considered as a quasi-neutral system consisting of electrons, ions, radicals, and excitations of gas molecules formed by the ionization and dissociation of gas molecules under external energy, such as an electric field. Using plasma, energetic electrons collide with the reactants and activate them, producing large quantities of highly reactive substances to initiate the reaction [11]. Thus, some stable small molecules, such as CH₄ [12–14], CO₂ [15–18] and N₂ [19,20], can be effectively activated by plasma. Compared with the traditional thermal activation of methane, plasma shows a strong activation ability on methane [21]. Methane and products can avoid deep oxidation reactions at low temperatures (lower than 600 °C), which is beneficial to the selectivity of C₂ hydrocarbon products. Therefore, research on the plasma activation of methane has become increasingly active in recent years. However, the gas-phase non-catalytic reaction initiated by plasma is mainly carried out through the free radical mechanism, which has little controllability of the product distribution [22].

To control the selectivity of products and enhance the performance of methane activation, catalysts are usually introduced into the plasma system. The addition of catalysts in the plasma can combine the characteristics of low-temperature activation of plasma with the characteristics of product orientation of the catalysts, which provides a high potential to produce value-added products. At present, several dielectric materials, such as TiO₂ [23], Al₂O₃ [24,25], SiO₂ [13,24], and ZSM [26,27], have been used for methane activation in the presence of plasma. Microelectrodes formed under an external electric field inside dielectric particles will enhance the electric field, thus improving the methane

conversion [24]. Moreover, the adsorption of porous material can also make the reactants relatively concentrated, which is expected to significantly improve the discharge energy efficiency [25,28]. Liu et al. [29] found that the presence of plasma vibrationally excited methane appeared to be primarily responsible for the improvement of methane conversion in the presence of catalysts. Vibrationally excited methane made a significant contribution to the formation of the products without catalysts, even though a large amount of electric field energy was consumed [30]. This was mainly due to the high internal energy; the vibrationally excited methane was more easily dissociated on the catalyst to produce methyl radicals, thus increasing the methane conversion. Therefore, the energy to overcome the methane activation barrier originates from the electric field rather than the external heat during the plasma reaction, thus avoiding the high-temperature condition.

In order to integrate the advantages of various catalysts, a more ideal approach is to form a composite of high-performance catalysts and dielectric materials. In this way, the local electric field generated by the high permittivity of catalysts can enhance the activation of methane, while simultaneously improving the selectivity of C₂ hydrocarbons [31,32]. However, so far, most of the studies on catalysts for methane oxidative coupling catalysts have been focused on thermal reactions at high temperatures, and few studies have reported their methane oxidation coupling activity under plasma conditions. Related studies have confirmed that catalysts with methane oxidation coupling performance at high temperatures also exhibit excellent OCM activity in the plasma [33]. Keller et al. [34] investigated the OCM activity of various metal oxides and found that manganese oxides presented excellent performance for C₂ formation with a low cost and environmental friendliness. Cheng et al. [35] employed Mg₆MnO₈ with the use of a low concentration of Li dopant as the catalyst for CL-OCM. The experiment showed that Mn-based oxides with Li dopant attained C₂ hydrocarbons with a selectivity of 50.4%. DFT calculations demonstrated that oxygen vacancies caused by Li-doping in Mg-Mn composite oxygen carriers were unfavorable for the adsorption of methyl radicals and, hence, increased the activation barrier of methyl radicals, thus significantly improving the selectivity of C₂ hydrocarbon. Jiang et al. [36] applied Na-doped LaMnO₃ as a catalyst in the CL-OCM process and found that Mn-based catalysts were well-suited catalysts, which could attain an ideal C₂ selectivity and yield. Moreover, Na₂WO₄ is considered as a suitable catalyst for the OCM reaction [37]. Previously, transition metal oxides impregnated with Na₂WO₄ were experimentally found to inhibit the formation of CO_x in the reaction, indicating that the introduction of Na₂WO₄ could result in the growth of C₂ selectivity [38]. Kiani et al. [39] prepared a Na₂WO₄/SiO₂ catalyst via a modified impregnation method and found that the OCM reaction occurred at the dispersed phase Na-WO₄ site. Due to the high thermal stability and superior C₂ yield, Mn/Na₂WO₄/SiO₂ is considered to be a promising catalyst to achieve commercial application [40,41]. Kim et al. [42] investigated the OCM activity of Mn/Na₂WO₄/TiO₂, and found that a superior C₂ yield was attained on Mn/Na₂WO₄/TiO₂ compared to on Mn/Na₂WO₄/SiO₂.

In this study, we investigated the effect of active metal loadings on different types of dielectric materials for methane conversion and C₂₊ production in dielectric barrier discharge (DBD) plasma at atmospheric pressure in chemical looping mode, with no oxygen co-feed. The regeneration process was carried out at 300 °C in an atmosphere of air under plasma. The impact of different input flows, temperatures, and applied voltages on the performance of the catalyst in the DBD reactor was also investigated. The catalysts were measured by X-ray diffraction (XRD) to confirm the crystal phases. H₂-temperature programmed reduction (H₂-TPR) and X-ray photoelectron spectroscopy (XPS) were performed to investigate the properties of oxygen species on catalysts. TEM-EDS was carried out to determine the element distributions. Finally, it was found that the MnTi catalyst resulted in a clear C₂₊ hydrocarbons enhancement in plasma when compared with a catalysis-only system. This discovery enables the room-temperature conversion of methane and provides an effective guideline for the study of methane activation in low-temperature plasma.

2. Results and Discussion

2.1. Effect of Dielectric Materials

All experiments were performed in chemical looping mode, meaning that no oxygen co-feed was present. The metal amount was not varied. According to the literature reported on plasma-catalytic systems, methane conversion and product selectivity would vary with different dielectric materials. It was found that the microelectrodes were generated inside the dielectric materials under the external electric field, which could improve the capability of charge transfer [43]. In terms of chemical reactions, the charge transfer capacity can be converted into the ability to activate methane, meaning that various dielectric materials can enhance the activity of methane conversion. Figure 2 shows the catalytic performance of SiO₂, Al₂O₃, and TiO₂ dielectric materials for CL-OCM in DBD plasma. SiO₂ exhibits the highest methane conversion of 37.75%, but contains CO and CO₂ as the main products (with a CO and CO₂ selectivity of 36.95% and 36.03%), resulting in a low C₂₊ yield of 9.12%, with a C₂₊ selectivity lower than 30%. While Al₂O₃ and TiO₂ exhibit an improvement for C₂₊ selectivity (mainly ethane and propane as the main products), C₂₊ yields of 9.85% and 11.63% are obtained, respectively. Compared to Al₂O₃, TiO₂ displays more remarkable oxidative coupling properties in plasma, which is illustrated by the further improvement in the selectivity of ethane and propane, and exhibits the highest C₂₊ yield among the used dielectric materials in this study. Thus, TiO₂ is considered as an ideal support for CL-OCM in plasma.

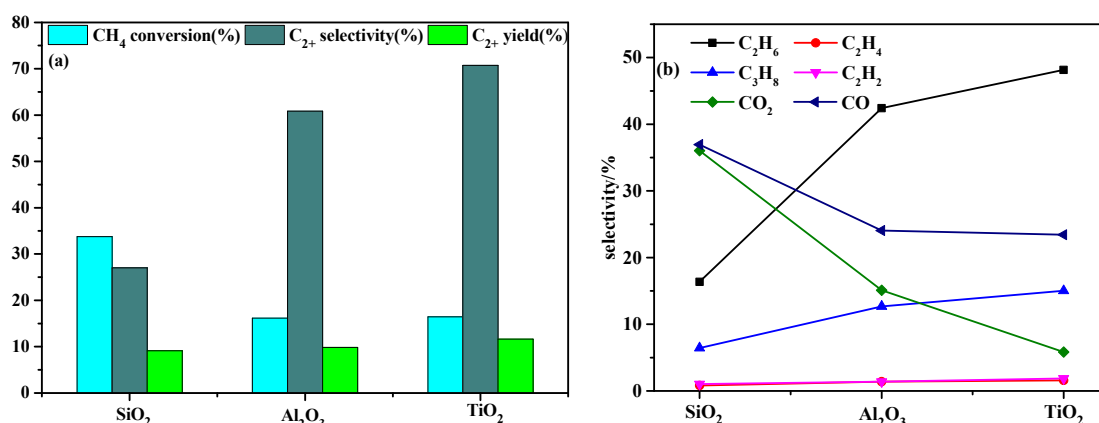


Figure 2. Performance of different dielectric materials in DBD plasma. (a) Oxidative coupling performance; (b) product distribution (temperature: ambient temperature, flow rate: 60 mL/min, applied voltage: 100 V).

In general, there is a positive correlation between the performance of catalysts and dielectric materials in the plasma-catalyst system. Since TiO₂ exhibited the best catalytic performance among the supports under plasma conditions, different metal loadings on TiO₂ support were further investigated. The catalytic performance of different metal loadings on TiO₂ support for CL-OCM in DBD plasma is shown in Figure 3. It can be seen that the loading of active metals on TiO₂ support contributes greatly to the increase in methane conversion and C₂₊ selectivity compared to pure TiO₂ in the plasma-catalytic system. The most striking improvement is nearly 100% of C₂₊ selectivity, with dominant products being ethane and propane, which account for more than 70% of the total products. As stated in previous research, manganese oxide and Na₂WO₄ would take part in the dehydrogenation reaction of methane and result in the formation of methyl radicals, which was the essential initial step in the OCM reaction [40,44,45]. However, a remarkable synergy between Mn(NO₃)₂ and Na₂WO₄ in the methane conversion could not be observed in the plasma system. The catalytic performance of different metal loadings on TiO₂ support in DBD plasma exhibits no obvious difference, and the order of activity of methane conversion and C₂₊ yield under different catalysts is MnTi > NaWTi > MNWTi. MnTi is chosen as the best catalyst judging from the C₂₊ yield.

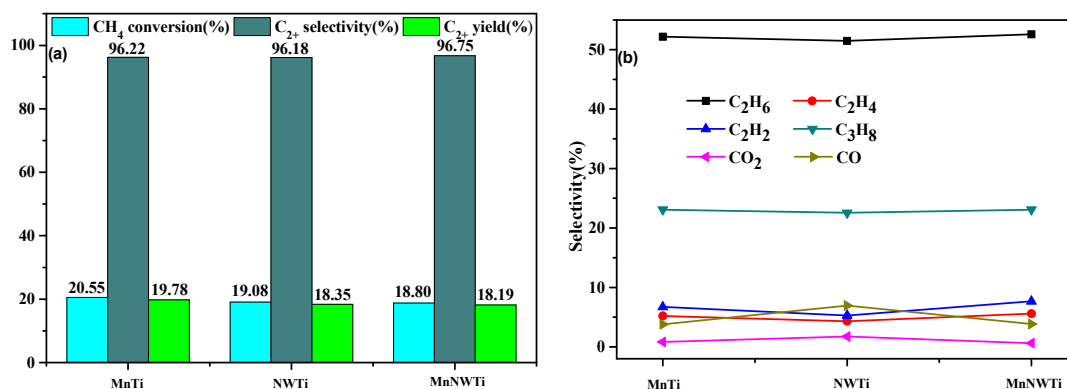


Figure 3. Performance of different metal loadings in DBD plasma. (a) Oxidative coupling performance; (b) product distribution (temperature: ambient temperature, flow rate: 60 mL/min, applied voltage: 100 V).

To investigate the role of plasma in methane conversion at low temperatures, comparison experiments were conducted, as shown in Figure 4. The C₂₊ yield of 19.78% can be obtained in the presence of plasma without additional thermal input, while the methane oxidative coupling performance of the MnTi catalyst is almost negligible, even at 850 °C on the MnTi catalyst without plasma. It generally known that C–H bond breakage of CH₄ cannot occur at ambient temperatures due to the high activation barrier; however, this can be enabled under plasma conditions. For the reaction under plasma conditions, electron collisions result in the formation of many excited state species with high internal energy. These excited state species have a lower C–H activation barrier, resulting in C–H breakage on the catalyst surface at a lower temperature. Thus, plasma plays a major role in activating the methane reaction, thus allowing the methane coupling reaction to occur at low temperatures.

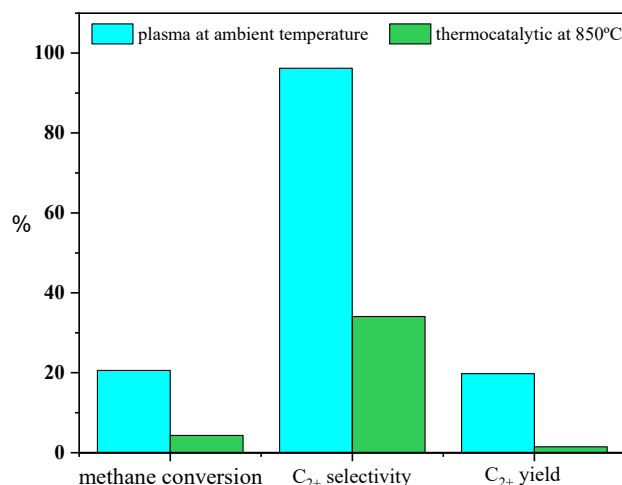


Figure 4. Catalytic performance of the MnTi catalyst with plasma and without plasma (flow rate: 60 mL/min, applied voltage: 100 V).

2.2. Effect of Flow Rate

Figure 5 shows the effect of different flow rates on the catalytic performance of the MnTi catalyst in the presence of DBD plasma. We can see that C₂₊ selectivity increases continuously with increasing input gas flow rate, but the selectivity of different products varies with the flow rate in a different trend. The selectivity of C₂H₄ and C₂H₂ increases with the increase in flow rate, while the selectivity of C₂H₆ and C₃H₈ remains stable. It is worth noting that the by-products of CO and CO₂ clearly decrease as the input flow increases, demonstrating the opposite effect of high input flow on C₂₊ selectivity. It could

be inferred that under the condition of a high input flow, the free radicals formed by the ionization of CH_4 molecules under an electric field are easier to desorb from the surface of the catalyst into the gas phase, and avoid the subsequent excessive oxidation, resulting in the improvement of C_{2+} selectivity. However, from Figure 5a it can also be seen that methane conversion decreases with the increase in input flow, which is mainly because the high space velocity decreases the gas residence time and the conversion [31,46,47]. A higher residence time would increase the probability of collision between methane and high-energy electrons, thus improving the conversion of methane. Comprehensively considering the methane conversion and C_{2+} selectivity, the flow rate of 60 mL/min is found to be the optimum flow rate on the MnTi catalyst. The methane conversion reaches a maximum of 20.72% and C_{2+} products achieve the highest yield of 20.03%.

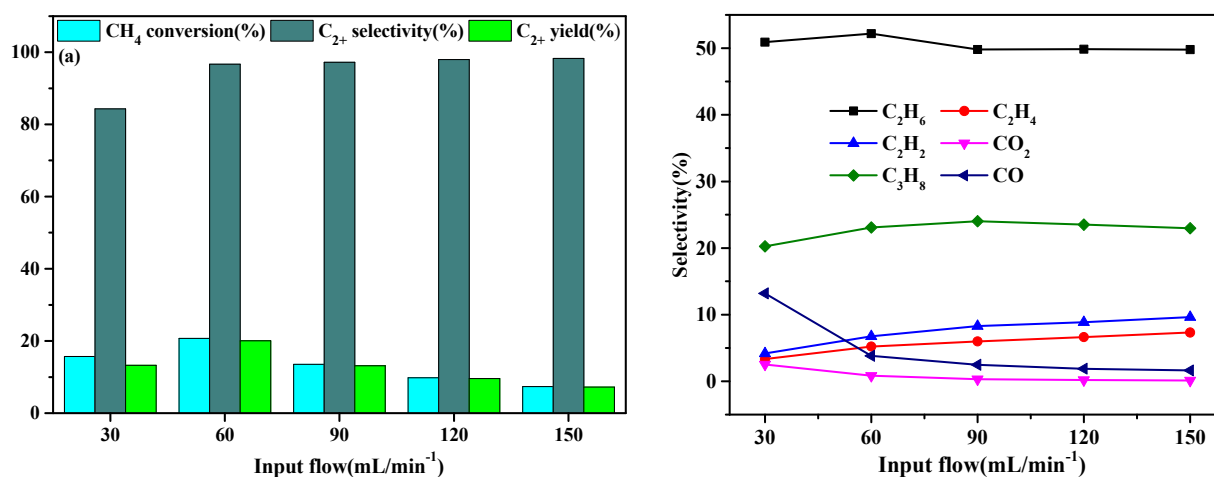


Figure 5. Effect of flow rate on the catalytic performance of the MnTi catalyst in DBD plasma. (a) Oxidative coupling performance; (b) product distribution (temperature: ambient temperature, applied voltage: 100 V).

2.3. Effect of Temperature

The variation of methane conversion and product selectivity with different temperatures is shown in Figure 6. A temperature of 200 °C is chosen as the upper limit to guarantee a reliable carbon balance. In light of the experimental results, the conversion of methane shows no significant difference. According to the previous literature, many efforts have been made to explore the effect of temperature on methane activation, but the relationship between temperature and catalytic performance is still controversial [33,34,48,49]. A similar result was observed by Liu et al., and the negative influence of temperature on methane conversion was attributed to the fact that a temperature rise favored the dehydration of the catalyst, which resulted in a decrease in OH^- concentration [33]. It was believed that hydroxyl species played a positive role in the activation of methane under an electric field. Similarly, from Figure 6b, it can also be found that the rise in temperature has little consequences for the distribution of the products. Therefore, the effect of temperature below 200 °C on methane conversion in DBD plasma can be considered negligible. This is because the dissociation energy of the C–H chemical bond is high up to 434 kJ/mol, which is almost impossible to be activated below 500 °C in traditional thermal reactions. Therefore, the breakage of the C–H bond in methane and subsequently generated methyl radicals is mainly initiated by high-energy electron collisions of plasma under 500 °C, rather than by additional thermal input.

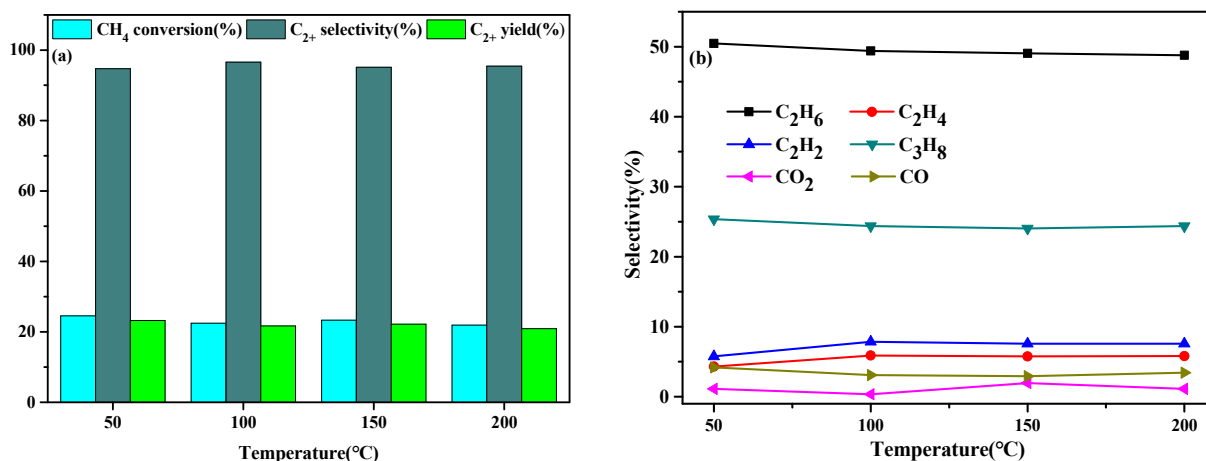


Figure 6. Effect of temperature on the catalytic performance of the MnTi catalyst in DBD plasma. (a) Oxidative coupling performance; (b) product distribution (flow rate: 60 mL/min, applied voltage: 100 V).

2.4. Effect of Applied Voltage

Figure 7 shows the catalytic performance of the MnTi catalyst in DBD plasma at different applied voltages, and 200 V is chosen as the upper limits to guarantee a reliable carbon balance. The conversion of methane increases with the increase in applied voltage. Lissajous plots of different applied voltages are shown in Figure 8, and the discharge power is calculated by the integral area of the Lissajous plots. According to the calculation, the increase in applied voltage will increase the discharge power, thus generating more high-energy electrons. The increased number of high-energy electrons may lead to a higher probability of bond breakage between carbon and hydrogen in the methane molecules, thus improving the degree of methane dissociation and conversion, which appears to be primarily responsible for a higher CH₄ activation [47]. However, the product distribution is independent of applied voltage and shows little difference with the variation of applied voltage, as shown in Figure 7b. Noticeably, the C₂₊ yield reaches a maximum of 30.04% at an applied voltage of 200 V, but the carbon balance of 85.28% is not perfect (the carbon balance of different applied voltages is displayed in Figure 9), indicating that the coke is formed due to methane cracking [31]. However, we still could obtain a 27.29% C₂₊ yield at a reliable carbon balance (91.4%) at 150 V applied voltage.

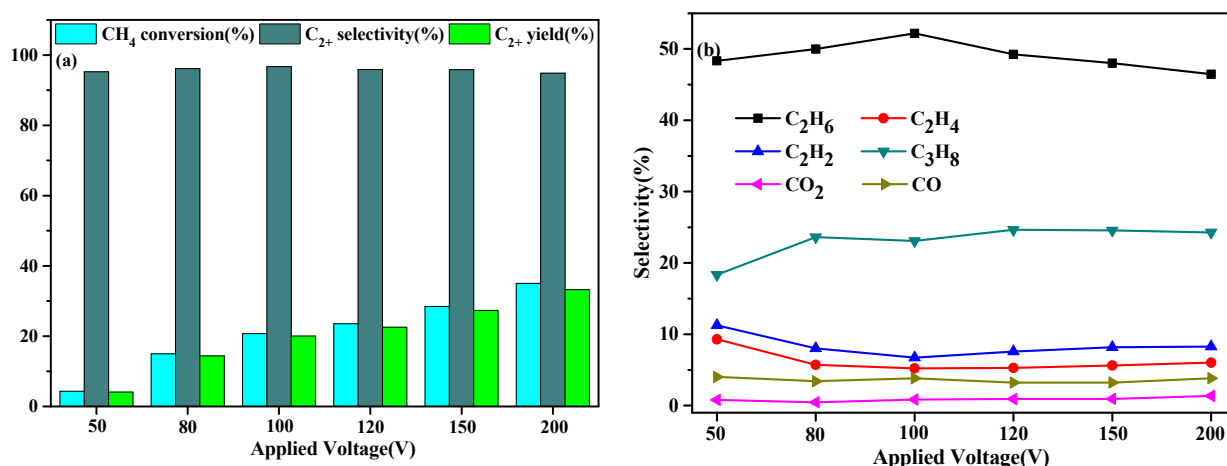


Figure 7. Effect of applied voltage on the catalytic performance of the MnTi catalyst in DBD plasma. (a) Oxidative coupling performance; (b) product distribution (temperature: ambient temperature, flow rate: 60 mL/min).

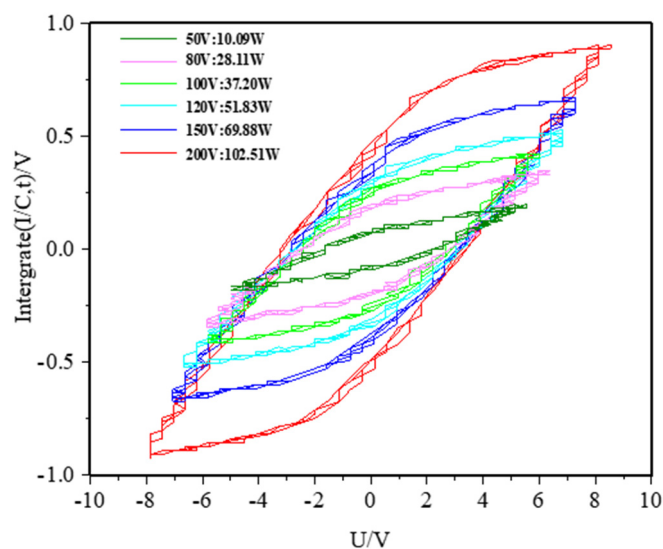


Figure 8. Lissajous plots of different applied voltages on the MnTi catalyst.

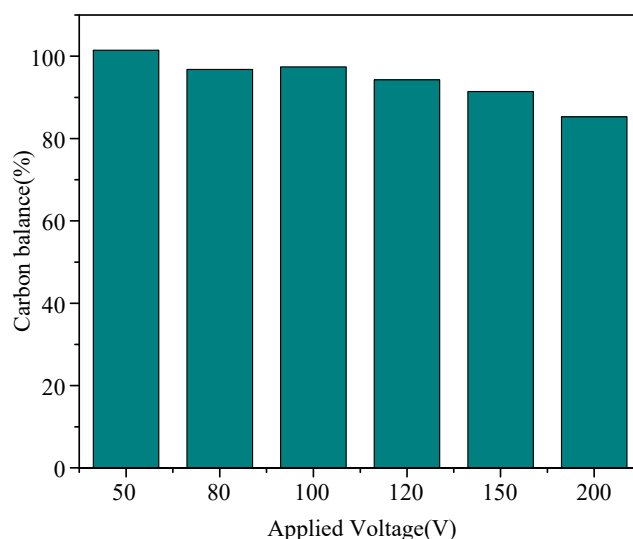


Figure 9. Carbon balance of different applied voltages on the MnTi catalyst.

3. Characterization

3.1. XRD

The XRD patterns of the as-prepared catalysts are shown in Figure 10. According to the XRD patterns, all the characteristic diffraction peaks of TiO_2 correspond well with the anatase phase in the JCPDS database (PDF-#84-1286). Moreover, new diffraction peaks also appear in the fresh MnTi catalyst with a structural change, indicating the emergence of a new phase after the loading of manganese nitrate. By comparing with the JCPDS database, these new diffraction peaks can be assigned to the rutile phase, which becomes the most dominant crystalline phase of the catalyst, judging from the intensity of the diffraction peaks. This change in crystalline phase structure is consistent with the thermal behavior of titanium dioxide [50]. The rutile phase is still the most dominant crystalline phase structure of the catalyst when the MnTi catalyst is reduced by CH_4 , confirming the stability of the catalyst structure. It is worth noting that no characteristic diffraction peak for Mn in XRD patterns is observed, which might be due to low Mn loading or the high dispersion of Mn in the catalyst.

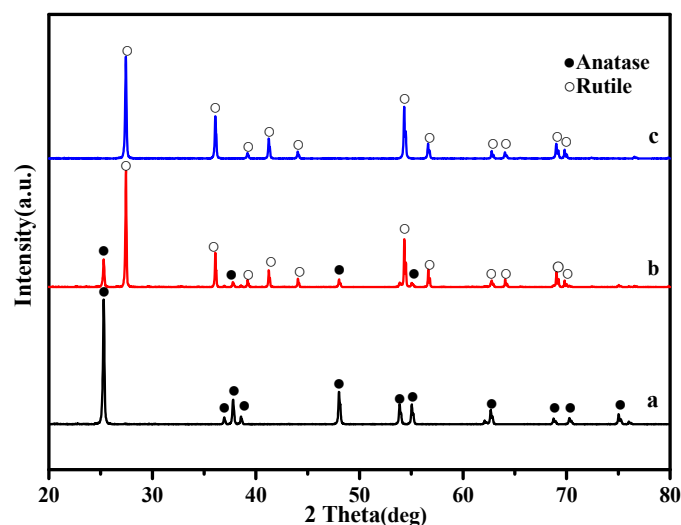


Figure 10. XRD patterns of (a) TiO_2 , (b) fresh MnTi catalyst, and (c) reduced MnTi catalyst.

3.2. XPS

According to previous research, oxygen species play an important role in the process of oxidative coupling of methane [48]. Thus, it is necessary to explore the oxygen species on the catalyst surface, which can further explain the reasons for the improvement in methane activation and C_2 hydrocarbon selectivity through the synergetic effects between the catalyst and the plasma. The surface compositions and chemical states of the oxygen species were explored by XPS measurements, as displayed in Figure 11. For each TiO_2 -based catalyst, four peaks are used for the fitting of the O 1s spectra. The peak at a lower binding energy between 528.69 eV and 529.61 eV is assigned to surface lattice oxygen (O^{2-}) [51]; the second peak existing between 531.65 eV and 529.68 eV is attributed to the surface adsorbed oxygen species (O_2^{2-} , O^-) [36]; the third peak with a binding energy of about 533.11–531.48 eV results from hydroxyl species OH^- [52]; and the fourth peak with a binding energy higher than 534.0 eV is ascribed to adsorbed molecular water species H_2O [52]. The composition of the surface O species is displayed in Table 1. Among them, lattice oxygen species are considered as non-selective oxygen species, which contribute to the complete oxidation of methane and the generation of CO_x by-products, thus limiting C_{2+} selectivity [36]. Compared with TiO_2 , it can be seen that Mn loading clearly increases the concentration of hydroxyl species, whilst simultaneously reducing the concentration of lattice oxygen. The decrease in lattice oxygen species indicates the increase in selective oxygen species, which favors the oxidative coupling of methane. Moreover, evidence from the literature also shows that hydroxyl species OH^- would react with different oxygen species to form catalytic active sites for OCM, which could significantly improve methane activation and C_2 selectivity. Moreover, the presence of hydroxyl species could create a micro-discharge on the catalyst surface, which further facilitates the activation of methane [30,33,45]. Compared to fresh MnTi catalyst, the concentration of the surface adsorbed oxygen species (O_2^{2-} , O^-) decreases after reduction with CH_4 , confirming that the surface adsorbed oxygen species (O_2^{2-} , O^-) takes part in the oxidative coupling of methane. Moreover, it can be observed that there is a peak shift of the oxygen species towards a low binding energy when compared to pure TiO_2 catalyst, indicating the improvement in oxygen mobility and the formation of oxygen vacancies on the MnTi catalyst. The existence of oxygen vacancies can reduce the adsorption energy of methyl radicals, thereby increasing the selectivity for C_{2+} hydrocarbons.

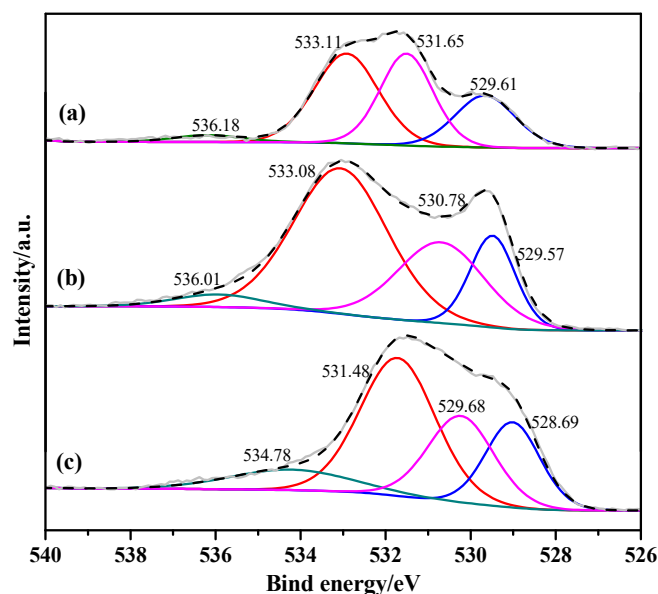


Figure 11. XPS scans on O 1s for (a) TiO₂, (b) fresh MnTi catalyst, and (c) reduced MnTi catalyst.

Table 1. Composition of the surface O species for fresh and spent MnTi catalyst and TiO₂.

Sample	Oxygen Distribution/%			
	O ²⁻	O ₂ ²⁻ /O ⁻	OH ⁻	H ₂ O
TiO ₂	21.94	37.96	36.05	4.06
Fresh 5%Mn(NO ₃) ₂ -TiO ₂	17.02	28.41	45.33	8.63
Reduced 5%Mn(NO ₃) ₂ -TiO ₂	17.82	22.73	49.26	10.18

3.3. TEM-EDS

TEM-EDS was carried out to explore the dispersion of Mn on the fresh MnTi catalyst, as displayed in Figure 12. The TEM images of the fresh MnTi catalyst reflect that Mn nanoparticles are dispersed uniformly on rod TiO₂ and no obvious Mn clusters can be found, confirming the high dispersion of Mn element on the catalyst surface. EDS mapping also demonstrates that Mn is distributed uniformly on the fresh MnTi catalyst. This explains the absence of Mn element in the XRD pattern. As stated in previous research, the stability and reaction activity of catalysts are closely related to the dispersion of the loaded metal. A higher dispersion of the metal would expose more active site edges or corners, which are more reactive on the metal surface, and hence be more conducive to improving the reactivity of the catalyst in different reactions [53]. Therefore, a higher Mn dispersion will be more favorable for the formation of C₂₊ hydrocarbons due to the large number of unsaturated active sites that are more active for the breakage of C-H bonds.

3.4. H₂-TPR

The reduction properties correlated with oxygen release characteristics of catalysts were tested by H₂-TPR technology, as shown in Figure 13. It can be observed that TiO₂ presents the low reductive property between 50 to 300 °C, and an obvious reduction peak of TiO₂ emerges from 300 °C and exhibits a peak at 625 °C, owing to the reduction of O₂²⁻ species at 387 °C and coordinatively unsaturated Ti³⁺ at 625 °C, respectively [51]. However, in the MnTi catalyst profile, a new reduction peak region emerges at ~551 °C, which contributes to the reduction process of Mn₂O₃ [36,54]. It was reported that Mn₂O₃ played a crucial role in enhancing the OCM activity of catalysts, which could take part in the hydrogen abstraction from CH₄ and trigger CH₄ activation. Moreover, the total reduction peak area increases as Mn is induced, confirming that the catalytic performance of the catalyst is enhanced. It is important to note that the reduction peaks of Ti³⁺ shift from

625 °C to 551 °C after Mn is loaded, demonstrating the improvement in oxygen release. This also proves, to some extent, that the formation of oxygen vacancies facilitates the formation of C₂ hydrocarbon products.

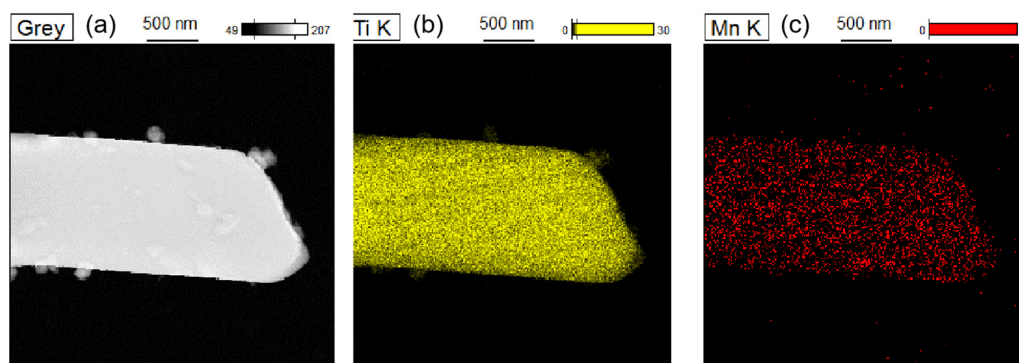


Figure 12. EDS mapping of the fresh MnTi catalyst (a) TEM images of MnTi catalyst, (b) Ti element distribution, and (c) Mn element distribution.

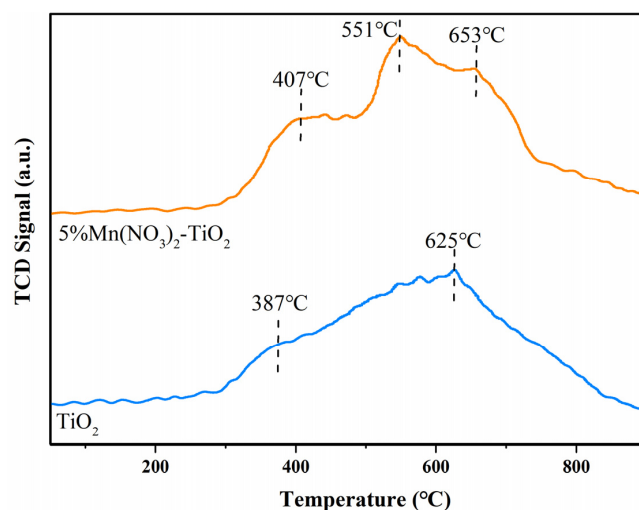


Figure 13. H₂-TPR profiles.

A possible reaction mechanism for CL-OCM on the MnTi catalyst is displayed in Figure 14. Because of the high relative permittivity, TiO₂ particles are polarized in the plasma discharge and a local electric field is formed around the particle contact point, causing an increase in methane conversion. Additionally, manganese oxide will take part in the hydrogen abstraction of methane, which is the first step of CL-OCM. In the traditional thermo-catalytic reaction, methane activation requires a high temperature due to the high activation barrier of the C-H bond. For the reaction in plasma, CH₄ activation is initiated by electronic collision to form substantial species, including radicals, ions, and vibrationally or electronically excited species. The existence of vibrationally excited methane appears to be primarily responsible for the improvement in methane conversion and C₂₊ selectivity in the presence of catalysts. Compared to the thermo-catalytic reaction, vibrationally excited methane molecules with elevated internal energy have a lower C-H activation barrier, and can, thereby, be activated on the Mn site at a much lower temperature, demonstrating that the combination of TiO₂ with the Mn species has a synergistic effect for CL-OCM reaction. Moreover, Mn loading can increase the amounts of hydroxyl species and oxygen vacancies, which can create a micro-discharge on the catalyst surface, thus facilitating the activation of methane. The increase in oxygen vacancies can reduce the adsorption energy of methyl radicals, thereby increasing the selectivity for C₂₊ hydrocarbons. It is

noteworthy that coking becomes severe with increasing reduction time, which indicates that the redox-active lattice is consumed relatively quickly.

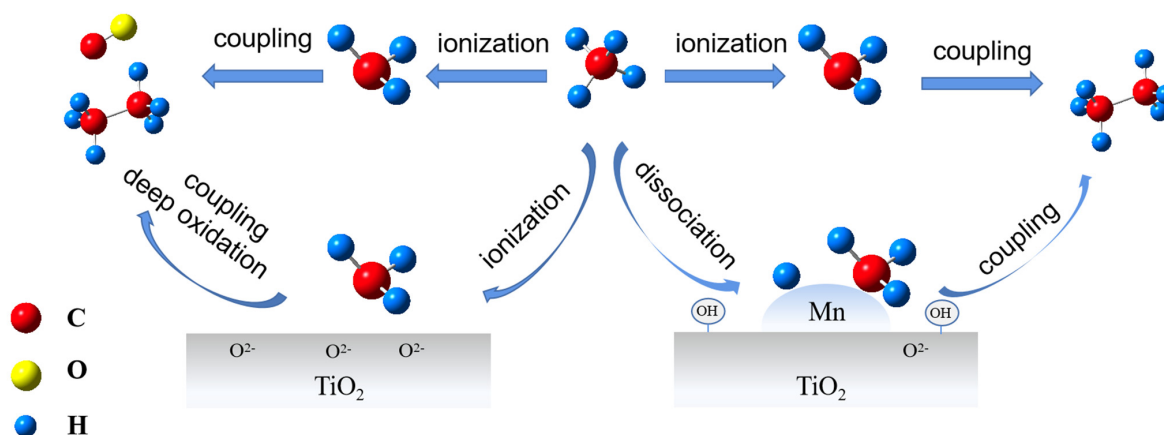


Figure 14. Possible reaction mechanism for CL-OCM on the MnTi catalyst.

3.5. Chemical Looping Redox Experiments

Since the stability and recyclability of catalysts are of utmost importance for catalysts in industrial chemical looping applications, 30 consecutive cyclic redox tests were explored on the MnTi catalyst. The catalytic performance of the catalyst on methane conversion, C_{2+} selectivity, and C_{2+} yield in the plasma–catalyst hybrid system is displayed in Figure 15. It can be seen that methane conversion and C_{2+} yield remain stable at average values of ~21% and ~20%, respectively, while the C_{2+} products selectivity simultaneously stays above 95% during 30 consecutive cyclic redox tests, demonstrating that the reactivity of the MnTi catalyst is fully recovered after the regeneration by plasma, and it presents good regeneration ability in the plasma–catalyst hybrid system. Moreover, compared to thermal regeneration, plasma regeneration could realize catalyst regeneration at a lower temperature (300 °C). According to relevant literature, the good regeneration of catalysts in plasma could be ascribed to the fact that reactive oxygen species were formed [48]. Reactive oxygen species, on the one hand, reacted more easily with carbon deposition to generate CO and CO_2 , avoiding catalyst deactivation; on the other hand, they oxidized the reduced catalyst to recover OCM performance.

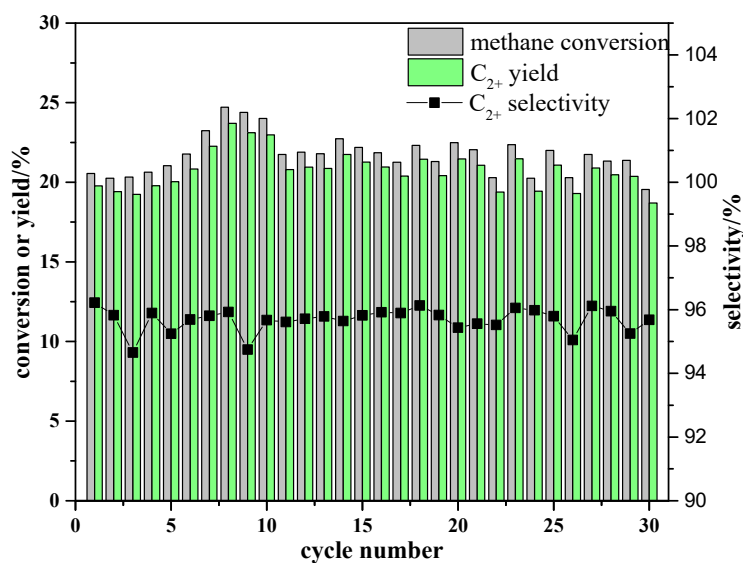


Figure 15. CLOCM of the MnTi catalyst (temperature: ambient temperature, flow rate: 60 mL/min, applied voltage: 100 V).

4. Experimental

4.1. Preparation of the Catalyst

5%Mn(NO₃)₂-TiO₂ (MnTi), 10%Na₂WO₄-TiO₂ (NWTi), and 5%Mn(NO₃)₂ + 10%Na₂WO₄-TiO₂ (MnNWTi) used in this study were prepared by the impregnation method, using aluminum oxide (Al₂O₃, Maclin), silica sand (SiO₂, 6–10 mesh, Maclin), anatase titanium oxide (TiO₂, 99.0% pure, Maclin), manganese nitrate hydrate (Mn(NO₃)₂, 50 wt% in water, Maclin), and sodium tungstate dihydrate (Na₂WO₄·2H₂O, 99.5% pure, Maclin). To obtain the MnTi catalyst, TiO₂ was impregnated with aqueous solutions of Mn(NO₃)₂ as precursors, yielding 5 wt% Mn(NO₃)₂, and then dried at 105 °C until the water evaporated completely. Finally, the catalyst was calcined at 850 °C for 6 h and the MnTi catalyst was obtained. The production process of MnNWTi and NWTi followed the same procedure as described above.

4.2. Material Characterization

The prepared catalysts were measured by X-ray diffraction (XRD) using a Japan Science D/max-R Diffractometer (Tokyo, Japan) with Cu K α radiation (40 kV, 40 mA, $\lambda = 0.15406$ nm) to confirm the structural features and crystal phases. The catalysts were scanned with a 2θ range of 10–80° at a rate of 10°/min.

The valence state of the oxygen species of fresh and reduced catalysts was investigated by X-ray photoelectron spectroscopy (ESCALAB 250Xi, Thermo Fisher Scientific Inc, Waltham, MA, USA) with an Al K α X-ray source ($h\nu = 1486.6$ eV) operating under the conditions of 20 kV and 10 mA.

The microstructure and lattice parameters of the catalyst were determined by transmission electron microscopy (JEO-2100F, JEOL, Akishima, Japan), and elemental distribution was confirmed by energy dispersive spectroscopy. Before analysis, the catalyst was treated in ethanol by ultrasonic dispersion for 20 min to obtain a uniform suspension.

H₂-temperature programmed reduction (H₂-TPR) technology was employed to determine the reducibility of catalysts with a Quantachrome ChemStar™ (Graz, Austria) instrument rigged with a thermal conductivity detector (TCD). Catalyst powder with a weight of 50 mg was loaded in a U-shape quartz tube. In order to remove water molecules and air molecules adsorbed on the catalyst surface, the catalyst was kept at 300 °C for 1 h under a helium atmosphere as a pretreatment. The heating rate of the catalysts was 10 °C/min and the flow rate of He carrier gas was 35 mL/min. After pretreatment, the catalyst was heated from 50 °C to 900 °C at a heating rate of 10 °C/min, in 10% H₂ and 90% Ar at a flow rate of 30 mL/min.

4.3. Catalytic Test

The CL-OCM experiment was tested with a plasma-catalytic DBD reactor system at atmospheric pressure, as displayed in Figure 16. The DBD reactor was an alumina tube (O.D: 25 mm, I.D: 20 mm) consisting of a stainless-steel rod as the inner electrode centered in the reactor. The high-frequency discharge probe of the plasma generator (CTP-2000K, Nanjing, China), whose panel could read the input voltage, and voltage regulator were directly connected to the stainless-steel rod, and the outer electrode was connected to the outer capacitor (or resistance). The discharge parameters were recorded using a digital oscilloscope (DPO 2024B, Tektronix) to draw Lissajous plots for the calculation of the output power of plasma. The calculation formula is as follows:

$$P(\text{out}) = f \times C \times k \times k_x \times k_y \times S$$

In this experiment, $f = 10.04$ kHz, $C = 0.47$ μ F, $k = 1000$, $k_x, k_y = 1$, and S is the integral area of the Lissajous plots.

The catalyst pellets with a particle size of 20–50 mesh (2.0 g) were charged into the stainless mesh (>300 mesh) at the bottom of the stainless-steel rod. The stainless-steel mesh was placed in the grid area outside the alumina tube to ensure that the catalyst was within

the discharge area. All experiments were conducted at atmospheric pressure. During the reaction step, the DBD reactor was set at the experimental temperature and pure N₂ was used for purging. The reaction gas (40% volume fraction CH₄, balance Ar) flowed through the reactor using a mass flow controller. After the introduction of CH₄, the plasma was turned on for 10 min and the gaseous products were collected. The regeneration process was carried out at 300 °C for 10 min in conditions of 21% O₂ balanced with N₂ under plasma with an applied voltage of 100 V. The gaseous products were analyzed by a gas chromatograph (GC-2014, Shimadzu in Japan).

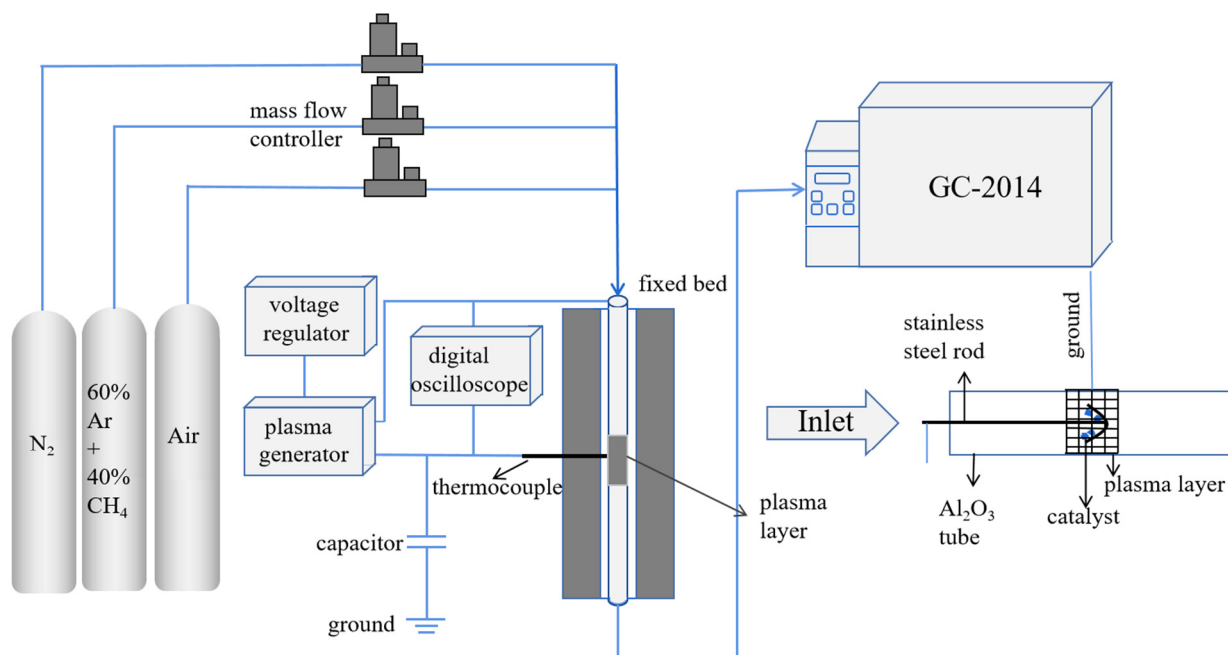


Figure 16. Reaction equipment diagram (the part on the bottom right is a magnification of the catalyst placement).

The conversion of methane, selectivity, and the yield of the C₂ product were determined by the following Equations (1)–(3):

$$X(\text{CH}_4)(\%) = \frac{\text{moles of CH}_4 \text{ converted}}{\text{moles of CH}_4 \text{ feed}} \times 100 \quad (1)$$

$$S(\text{C}_x)(\%) = \frac{x \times \text{moles of C}_x \text{ produced}}{\text{moles of CH}_4 \text{ converted}} \times 100 \quad (2)$$

$$Y(\text{C}_x)(\%) = \frac{x \times \text{moles of C}_x \text{ produced}}{\text{moles of CH}_4 \text{ feed}} \times 100 \quad (3)$$

5. Conclusions

In this study, the catalytic performance of different dielectric materials on methane oxidative coupling reaction was investigated in a DBD reactor. TiO₂ presented the best methane coupling performance among the various dielectric materials studies, such as SiO₂, Al₂O₃, and TiO₂. Hence, different active metal loadings on TiO₂ were tested. In light of the experimental results, metal loadings were capable of increasing methane conversion while simultaneously improving the C₂₊ selectivity. Among all tested catalysts, the MnTi catalyst was considered as the desirable catalyst judging from methane conversion and C₂₊ production. The high Mn dispersion, which was more conducive to improving the reactivity of the catalyst, was confirmed by TEM–EDS and XRD analysis. Moreover, the XPS spectra for O 1s revealed that Mn loading increased the concentration of hydroxyl

species and reduced the concentration of non-selective oxygen species, which resulted in the growth of methane conversion and C₂₊ selectivity. Finally, H₂-TPR spectra showed that Mn loading supplied more oxygen species, which was also beneficial for the formation of methyl radicals and C₂₊ hydrocarbons.

We further optimized various operation parameters to explore the OCM activity of the MnTi catalyst in plasma under different flow rates, applied voltages, and temperatures. A higher methane conversion was realized by increasing applied voltage and lowering flow rates. Moreover, the variation of operation parameters showed little effect on the product distribution, indicating that the selectivity of products was mainly affected by the properties of the catalysts rather than the operation parameters. Finally, excellent regenerative properties of the MnTi catalyst during chemical looping were confirmed through 30 consecutive cyclic redox tests, showing a methane conversion of about 21%, a 96% C₂₊ hydrocarbons selectivity, and a 20% C₂₊ hydrocarbon yield. Overall, the combination of TiO₂ with a high Mn metal dispersion in plasma reactors shows excellent OCM activity, which is a novel technology that achieves high catalytic properties and recyclability in methane oxidation coupling reactions.

Author Contributions: S.K.: Data curation, Formal analysis, Writing—original draft. J.D.: Data curation. X.W.: Writing—Review and editing. K.Z.: Conceptualization, Methodology, Funding acquisition, Writing—review and editing. M.Z.: Data curation. D.S.: Formal analysis. Z.H.: Writing—Review and editing. Y.L.: Formal analysis. A.L.: Formal analysis. A.Z.: Writing—Review and editing. Z.Z.: Writing—Review and editing. All authors have read and agreed to the published version of the manuscript.

Funding: This research was funded by the National Natural Science Foundation of China (51876205, 22279144, 51866003); the Youth Innovation Promotion Association, CAS (2019341); and the Yunnan Basic Research Program Project (2019FB071).

Data Availability Statement: Not applicable.

Conflicts of Interest: There is no conflict of interest.

References

1. Boswell, R. Is gas hydrate energy within reach? *Science* **2009**, *325*, 957–958. [[CrossRef](#)] [[PubMed](#)]
2. McFarland, E. Unconventional chemistry for unconventional natural gas. *Science* **2012**, *338*, 340–342. [[CrossRef](#)] [[PubMed](#)]
3. Gu, H.; Gao, Y.; Iftikhar, S.; Li, F. Ce stabilized Ni–SrO as a catalytic phase transition sorbent for integrated CO₂ capture and CH₄ reforming. *J. Mater. Chem. A* **2022**, *10*, 3077–3085. [[CrossRef](#)]
4. Yuan, K.; Wang, Y.; Li, K.; Zhu, X.; Wang, H.; Jiang, L.; Wei, Y.; Shan, S.; Zheng, Y. LaFe_{0.8}Co_{0.15}Cu_{0.05}O₃ Supported on Silicalite-1 as a Durable Oxygen Carrier for Chemical Looping Reforming of CH₄ Coupled with CO₂ Reduction. *ACS Appl. Mater. Interfaces* **2022**, *14*, 39004–39013. [[CrossRef](#)]
5. Li, Z.; Feng, X.; Gu, Z.; Lu, C.; Li, D.; Zhu, X.; Jiang, L.; Deng, G.; Li, K. Enhanced performance of the CeO₂MgO oxygen carrier by NiO for chemical looping CO₂ splitting. *Fuel Process. Technol.* **2022**, *225*, 107045. [[CrossRef](#)]
6. Holmen, A. Direct conversion of methane to fuels and chemicals. *Catal. Today* **2009**, *142*, 2–8. [[CrossRef](#)]
7. Hou, Y.; Han, W.; Xia, W.; Wan, H. Structure Sensitivity of La₂O₂CO₃ Catalysts in the Oxidative Coupling of Methane. *ACS Catal.* **2015**, *5*, 1663–1674. [[CrossRef](#)]
8. Wang, H.; Schmack, R.; Paul, B.; Albrecht, M.; Sokolov, S.; Rümmler, S.; Kondratenko, E.V.; Kraehnert, R. Porous silicon carbide as a support for Mn/Na/W/SiC catalyst in the oxidative coupling of methane. *Appl. Catal. A-Gen.* **2017**, *537*, 33–39. [[CrossRef](#)]
9. Zhang, Z.; Ji, S.F. Numerical simulation of particle/monolithic two-stage catalyst bed reactor with beds-interspace distributed dioxygen feeding for oxidative coupling of methane. *Comput. Chem. Eng.* **2016**, *90*, 247–259. [[CrossRef](#)]
10. Guo, X.; Fang, G.; Li, G.; Ma, H. Direct, nonoxidative conversion of methane to ethylene, aromatics, and hydrogen. *Science* **2014**, *344*, 616–619. [[CrossRef](#)]
11. Goujard, V.; Tatibouët, J.-M.; Batiot-Dupeyrat, C. Carbon Dioxide Reforming of Methane Using a Dielectric Barrier Discharge Reactor: Effect of Helium Dilution and Kinetic Model. *Plasma Chem. Plasma Process.* **2011**, *31*, 315–325. [[CrossRef](#)]
12. Hu, X.; Liu, Y.; Dou, L.; Zhang, C.; Zhang, S.; Gao, Y.; Tu, X.; Shao, T. Plasma enhanced anti-coking performance of Pd/CeO₂ catalysts for the conversion of methane. *Sustain. Energy Fuels* **2022**, *6*, 98–109. [[CrossRef](#)]
13. Kim, J.; Go, D.B.; Hicks, J.C. Synergistic effects of plasma-catalyst interactions for CH₄ activation. *Phys. Chem. Chem. Phys.* **2017**, *19*, 13010–13021. [[CrossRef](#)] [[PubMed](#)]
14. Guo, Z.; Yi, Y.; Wang, L.; Yan, J.; Guo, H. Pt/TS-1 Catalyst Promoted C–N Coupling Reaction in CH₄–NH₃ Plasma for HCN Synthesis at Low Temperature. *ACS Catal.* **2018**, *8*, 10219–10224. [[CrossRef](#)]

15. Bogaerts, A.; Berthelot, A.; Heijkers, S.; Kolev, S.; Snoeckx, R.; Sun, S.; Trenchev, G.; Van Laer, K.; Wang, W. CO₂ conversion by plasma technology: Insights from modeling the plasma chemistry and plasma reactor design. *Plasma Sources Sci. Technol.* **2017**, *26*, 063001. [[CrossRef](#)]
16. Debek, R.; Azzolina-Jury, F.; Travert, A.; Mauge, F. A review on plasma-catalytic methanation of carbon dioxide—Looking for an efficient catalyst. *Renew. Sustain. Energy Rev.* **2019**, *116*, 109427. [[CrossRef](#)]
17. Liu, J.L.; Wang, X.; Li, X.S.; Likozar, B.; Zhu, A.M. CO₂ conversion, utilisation and valorisation in gliding arc plasma reactors. *J. Phys. D Appl. Phys.* **2020**, *53*, 253001. [[CrossRef](#)]
18. Qin, Y.; Niu, G.H.; Wang, X.; Luo, D.B.; Duan, Y.X. Status of CO₂ conversion using microwave plasma. *J. CO₂ Util.* **2018**, *28*, 283–291. [[CrossRef](#)]
19. Barboun, M.; Mehta, P.; Herrera, F.; Go, D.; Schneider, W. Distinguishing Plasma Contributions to Catalyst Performance in Plasma-Assisted Ammonia Synthesis. *ACS Sustain. Chem. Eng.* **2019**, *7*, 32. [[CrossRef](#)]
20. Zhu, X.B.; Liu, J.; Hu, X.L.; Zhou, Z.J.; Li, X.B.; Wang, W.T.; Wu, R.B.; Tu, X. Plasma-catalytic synthesis of ammonia over Ru-based catalysts: Insights into the support effect. *J. Energy Inst.* **2022**, *102*, 240–246. [[CrossRef](#)]
21. Xu, C.; Tu, X. Plasma-assisted methane conversion in an atmospheric pressure dielectric barrier discharge reactor. *J. Energy Chem.* **2013**, *22*, 420–425. [[CrossRef](#)]
22. Thanyachotpaiboon, K.; Chavadej, S.; Caldwell, T.A. Conversion of Methane to Higher Hydrocarbons in AC Nonequilibrium Plasmas. *AIChE J.* **2010**, *44*, 2252–2257. [[CrossRef](#)]
23. Bouchoul, N.; Fourré, E.; Duarte, A.; Tanchoux, N.; Louste, C.; Batiot-Dupeyrat, C. Plasma-metal oxides coupling for CH₄-CO₂ transformation into syngas and/or hydrocarbons, oxygenates. *Catal. Today* **2021**, *369*, 62–68. [[CrossRef](#)]
24. Kim, J.; Jeoung, J.; Jeon, J.; Kim, J.; Mok, Y.S.; Ha, K.S. Effects of dielectric particles on non-oxidative coupling of methane in a dielectric barrier discharge plasma reactor. *Chem. Eng. J.* **2019**, *377*, 119896. [[CrossRef](#)]
25. Bouchoul, N.; Touati, H.; Fourré, E.; Clacens, J.-M.; Batonneau-Gener, I.; Batiot-Dupeyrat, C. Plasma-catalysis coupling for CH₄ and CO₂ conversion over mesoporous macroporous Al₂O₃: Influence of the physico-chemical properties. *Appl. Catal. B-Environ.* **2021**, *295*, 120262. [[CrossRef](#)]
26. Han, Q.; Tanaka, A.; Matsumoto, M.; Endo, A.; Kubota, Y.; Inagaki, S. Conversion of methane to C₂ and C₃ hydrocarbons over TiO₂/ZSM-5 core-shell particles in an electric field. *RSC Adv.* **2019**, *9*, 34793–34803. [[CrossRef](#)] [[PubMed](#)]
27. Krawczyk, K.; Młotek, M.; Ulejczyk, B.; Schmidt-Szałowski, K. Methane conversion with carbon dioxide in plasma-catalytic system. *Fuel* **2014**, *117*, 608–617. [[CrossRef](#)]
28. Zhang, X.; Liu, Y.; Zhang, M.; Yu, T.; Chen, B.; Xu, Y.; Crocker, M.; Zhu, X.; Zhu, Y.; Wang, R.; et al. Synergy between β-Mo₂C Nanorods and Non-thermal Plasma for Selective CO₂ Reduction to CO. *Chem* **2020**, *6*, 3312–3328. [[CrossRef](#)]
29. Liu, L.; Das, S.; Zhang, Z.; Kawi, S. Nonoxidative Coupling of Methane over Ceria-Supported Single-Atom Pt Catalysts in DBD Plasma. *ACS Appl. Mater. Interfaces* **2022**, *14*, 5363–5375. [[CrossRef](#)]
30. Takanabe, K.; Iglesia, E. Rate and selectivity enhancements mediated by OH radicals in the oxidative coupling of methane catalyzed by Mn/Na₂WO₄/SiO₂. *Angew. Chem. Int. Ed. Engl.* **2008**, *47*, 7689–7693. [[CrossRef](#)]
31. Kasinathan, P.; Park, S.; Choi, W.; Hwang, Y.K.; Chang, J.S.; Park, Y.K. Plasma-Enhanced Methane Direct Conversion over Particle-Size Adjusted MO_x/Al₂O₃ (M = Ti and Mg) Catalysts. *Plasma Chem. Plasma Process.* **2014**, *34*, 1317–1330. [[CrossRef](#)]
32. Kim, S.S.; Kwon, B.; Kim, J. Plasma catalytic methane conversion over sol-gel derived Ru/TiO₂ catalyst in a dielectric-barrier discharge reactor. *Catal. Commun.* **2007**, *8*, 2204–2207. [[CrossRef](#)]
33. Liu, C.; Marafee, A.; Mallinson, R.; Lobban, L. Methane conversion to higher hydrocarbons in a corona discharge over metal oxide catalysts with OH groups. *Appl. Catal. A-Gen.* **1997**, *164*, 21–33. [[CrossRef](#)]
34. Keller, G.E.; Bhasin, M.M. Synthesis of ethylene via oxidative coupling of methane: I. Determination of active catalysts. *J. Catal.* **1982**, *73*, 9–19. [[CrossRef](#)]
35. Cheng, Z.; Baser, D.S.; Nadgouda, S.G.; Qin, L.; Fan, J.A.; Fan, L.-S. C₂ Selectivity Enhancement in Chemical Looping Oxidative Coupling of Methane over a Mg–Mn Composite Oxygen Carrier by Li-Doping-Induced Oxygen Vacancies. *ACS Energy Lett.* **2018**, *3*, 1730–1736. [[CrossRef](#)]
36. Jiang, S.C.; Ding, W.X.; Zhao, K.; Huang, Z.; Wei, G.Q.; Feng, Y.Y.; Lv, Y.J.; He, F. Enhanced Chemical looping oxidative coupling of methane by Na-doped LaMnO₃ redox catalysts. *Fuel* **2021**, *299*, 120932. [[CrossRef](#)]
37. Zeng, D.; Wang, C.; Liu, T.; Ou, W.; Xiao, R. Enhanced performance of chemical looping methane oxidative coupling by the synergistic effect of TiO₂ doped Na₂WO₄/Mn₂O₃/SiO₂ oxygen carriers. *Fuel Process. Technol.* **2022**, *234*, 107320. [[CrossRef](#)]
38. Lunsford, J.H. The catalytic oxidative coupling of methane. *Angew. Chem. Int. Ed. Engl.* **1995**, *34*, 970–980. [[CrossRef](#)]
39. Kiani, D.; Sourav, S.; Wachs, I.E.; Baltrusaitis, J. Synthesis and molecular structure of model silica-supported tungsten oxide catalysts for oxidative coupling of methane (OCM). *Catal. Sci. Technol.* **2020**, *10*, 3334–3345. [[CrossRef](#)]
40. Elkins, T.; Hagelin-Weaver, H. Characterization of Mn–Na₂WO₄/SiO₂ and Mn–Na₂WO₄/MgO catalysts for the oxidative coupling of methane. *Appl. Catal. A-Gen.* **2015**, *497*, 96–106. [[CrossRef](#)]
41. Arndt, S.; Otremba, T.; Simon, U.; Yildiz, M.; Schubert, H.; Schomäcker, R. Mn–Na₂WO₄/SiO₂ as catalyst for the oxidative coupling of methane. What is really known? *Appl. Catal. A-Gen.* **2012**, *425*, 53–61. [[CrossRef](#)]
42. Kim, G.J.; Aussenbaugh, J.T.; Hwang, H.T. Effect of TiO₂ on the Performance of Mn/Na₂WO₄ Catalysts in Oxidative Coupling of Methane. *Ind. Eng. Chem. Res.* **2021**, *60*, 3914–3921. [[CrossRef](#)]

43. Chen, H.; Lee, H.; Chen, S.; Chao, Y.; Chang, M. Review of plasma catalysis on hydrocarbon reforming for hydrogen production—Interaction, integration, and prospects. *Appl. Catal. B-Environ.* **2008**, *85*, 1–9. [[CrossRef](#)]
44. Hou, S.; Cao, Y.; Xiong, W.; Liu, H. Site requirements for the oxidative coupling of methane on SiO₂-supported Mn catalysts. *Ind. Eng. Chem. Res.* **2006**, *45*, 7077–7083. [[CrossRef](#)]
45. Chawdhury, P.; Bhargavi, K.; Subrahmanyam, C. A single-stage partial oxidation of methane to methanol: A step forward in the synthesis of oxygenates. *Sustain. Energy Fuels* **2021**, *5*, 3351–3362. [[CrossRef](#)]
46. Seyed, M.N.; Savadkoohi, H.A.; Feizabadi, S.Y. Methane Conversion to C2 Hydrocarbons Using Dielectric-barrier Discharge Reactor: Effects of System Variables. *Plasma Chem. Plasma Process.* **2008**, *28*, 189–202. [[CrossRef](#)]
47. Miao, Y.; Kreider, P.; Reddick, I.; Pommerenck, J.; Collin, R.; AuYeung, N.; von Jouanne, A.; Jovanovic, G.; Yokochi, A. Methane Coupling to Ethylene and Longer-Chain Hydrocarbons by Low-Energy Electrical Discharge in Microstructured Reactors. *Ind. Eng. Chem. Res.* **2021**, *60*, 6950–6958. [[CrossRef](#)]
48. Lee, H.; Lee, D.H.; Ha, J.M.; Kim, D.H. Plasma assisted oxidative coupling of methane (OCM) over Ag/SiO₂ and subsequent regeneration at low temperature. *Appl. Catal. A-Gen.* **2018**, *557*, 39–45. [[CrossRef](#)]
49. Huu, P.; Gil, S.; Patrick, D.; Anne, G.-F.; Khacef, A. Plasma-catalytic hybrid reactor: Application to methane removal. *Catal. Today* **2015**, *257*, 86–92.
50. Gunawidjaja, R.; Anderson, B.; Eilers, H. Structural and spectroscopic characterization of irreversible phase changes in rapidly heated precursors of europium-doped titania nanoparticles. *J. Solid State Chem.* **2018**, *258*, 15–23. [[CrossRef](#)]
51. Zhang, P.; Xiong, J.; Wei, Y.C.; Li, Y.F.; Zhang, Y.L.; Tang, J.J.; Song, W.Y.; Zhao, Z.; Liu, J. Exposed {0 0 1} facet of anatase TiO₂ nanocrystals in Ag/TiO₂ catalysts for boosting catalytic soot combustion: The facet-dependent activity. *J. Catal.* **2021**, *398*, 109–122. [[CrossRef](#)]
52. Zhao, K.; Li, L.W.; Zheng, A.Q.; Huang, Z.; He, F.; Shen, Y.; Wei, G.Q.; Li, H.B.; Zhao, Z.L. Synergistic improvements in stability and performance of the double perovskite-type oxides La₂–xSrxFeCoO₆ for chemical looping steam methane reforming. *Appl. Energy* **2017**, *197*, 393–404. [[CrossRef](#)]
53. Xie, P.; Pu, T.; Nie, A.; Hwang, S.; Purdy, S.C.; Yu, W.; Su, D.; Miller, J.T.; Wang, C. Nanoceria-Supported Single-Atom Platinum Catalysts for Direct Methane Conversion. *ACS Catal.* **2018**, *8*, 4044–4048. [[CrossRef](#)]
54. Yang, N.Z.; Guo, R.T.; Pan, W.G.; Chen, Q.L.; Wang, Q.S.; Lu, C.Z. The promotion effect of Sb on the Na resistance of Mn/TiO₂ catalyst for selective catalytic reduction of NO with NH₃. *Fuel* **2016**, *169*, 87–92. [[CrossRef](#)]

Disclaimer/Publisher’s Note: The statements, opinions and data contained in all publications are solely those of the individual author(s) and contributor(s) and not of MDPI and/or the editor(s). MDPI and/or the editor(s) disclaim responsibility for any injury to people or property resulting from any ideas, methods, instructions or products referred to in the content.